ACS APPLIED MATERIALS & INTERFACES

Research Article

www.acsami.org

Light-Responsive Plasmonic Arrays Consisting of Silver Nanocubes and a Photoisomerizable Matrix

Petr A. Ledin,[†] Michael Russell,[†] Jeffrey A. Geldmeier,[†] Ihor M. Tkachenko,[‡] Mahmoud A. Mahmoud,[§] Valery Shevchenko,[‡] Mostafa A. El-Sayed,[§] and Vladimir V. Tsukruk*,[†]

[†]School of Materials Science and Engineering and [§]Laser Dynamics Laboratory, School of Chemistry and Biochemistry, Georgia Institute of Technology, Atlanta, Georgia 30332, United States

[‡]Institute of Macromolecular Chemistry, National Academy of Sciences of Ukraine, Kharkovskoe shosse 48, Kiev 02160, Ukraine

Supporting Information

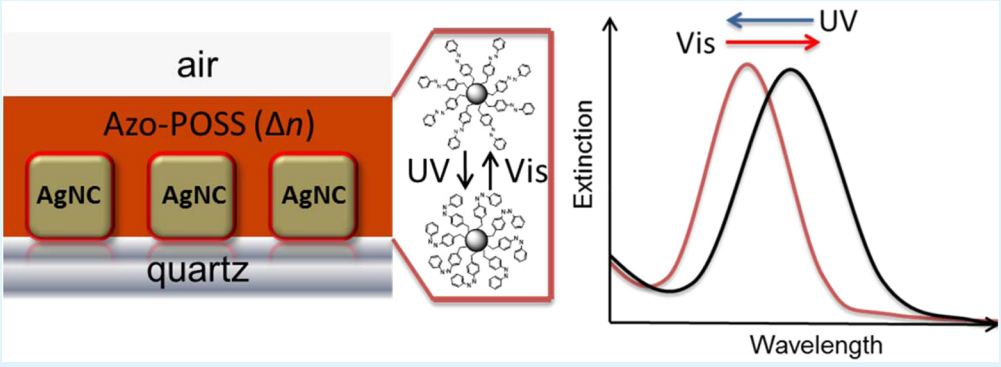

ABSTRACT: We report on the synthesis of novel branched organic−inorganic azo-polyhedral oligomeric silsesquioxane (POSS) conjugates (Azo-POSS) and their use as a stable active medium to induce reversible plasmonic modulations of embedded metal nanostructures. A dense monolayer of silver nanocubes was deposited on a quartz substrate using the Langmuir−Blodgett technique and subsequently coated with an ultrathin Azo-POSS layer. The reversible light-induced photoisomerization between the trans and cis states of the azobenzene-terminated branched POSS material results in significant changes in the refractive index (up to 0.17) at a wavelength of 380 nm. We observed that the pronounced and reversible change in the surrounding refractive index results in a corresponding hypsochromic plasmonic shift of 6 nm in the plasmonic band of the embedded silver nanocubes. The reversible tuning of the plasmonic modes of noble-metal nanostructures using a variable-refractive-index medium opens up the possibility of fabricating photoactive, hybrid, ultrathin coatings with robust, real-time, photoinitiated responses for prospective applications in photoactive materials that can be reversibly tuned by light illumination.

KEYWORDS: *plasmonic phenomena, azobenzene conjugates, polyhedral oligomeric silsesquioxane, photoisomerization*

INTRODUCTION

Noble-metal nanoparticles, especially those made of gold, silver, and platinum, have found many applications related to light−matter interactions such as photovoltaics,[1,2] catalysts,[3] solar concentrators, and surface-enhanced Raman scattering (SERS) sensors.[4,5] The nanoscale light confinement in surface plasmon (SP) modes can be used to design optical plasmonic waveguides, switches, and light-conversion materials and also facilitates the miniaturization of optoelectronic circuits.[6,7] The localized surface plasmon resonance (LSPR) is characteristic of nanoparticles with dimensions smaller than the wavelength of light and is extremely sensitive to nanoparticle material, shape, size, and coupling between nanoparticles as well as the dielectric environment surrounding the nanoparticle.[8] The coupling between metallic nanostructures can lead to their hybridization and a strong electromagnetic field enhancement in the interparticle gap.[9] This effect is particularly useful in sensing and photoenhancement.[10,11] Furthermore, by changing the refractive index of the dielectric environment surrounding the nanoparticle, it is possible to modulate the plasmonic characteristics, which opens up the possibility of fabricating active plasmonic devices with real-time responses.[12,13]

The most promising approach for creating a variable-refractive-index environment is the use of stimuli-responsive polymeric materials.[14] For instance, the transition between the hydrophilic swollen state and hydrophobic collapsed state of polymers such as poly(*N*-isopropylacrylamide) (PNIPAM) upon heating and cooling across the lower critical solution temperature (LCST) results in a change in the local refractive index of the polymer matrix.[15−20] Furthermore, refractive index changes can be observed in pH-responsive polymers such as poly(acrylic acid) (PAA), poly(2-vinylpyridine) (P2VP), and

Received: December 20, 2014
Accepted: February 11, 2015
Published: February 11, 2015

DOI: 10.1021/am508993z
ACS Appl. Mater. Interfaces 2015, 7, 4902−4912

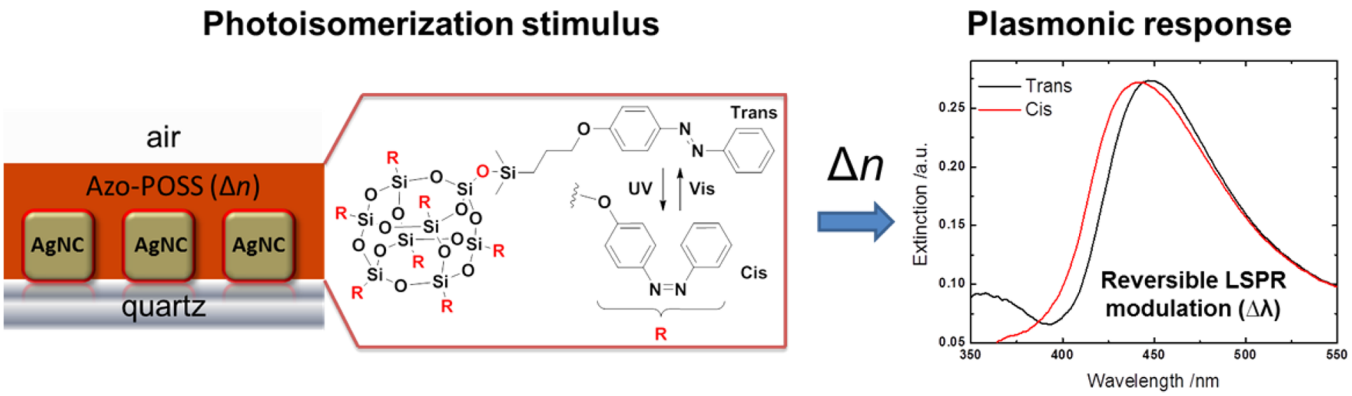

Figure 1. Branched Azo-POSS conjugates as a variable-refractive-index matrix for plasmonic nanoparticles.

poly(methacrylic acid) (PMAA).[21,22] With pH-responsive polymers, the LSPR shift and damping can be controlled by both the alteration of interparticle distance, and hence coupling, and the change in the refractive index as the polymer matrix swells in response to protonation or deprotonation.[23,24] Electrochromism of organic molecules and polymers induced by both chemical and electrochemical redox stimuli can also change the refractive index environment.[13,25,26]

A combination of responsive materials with plasmonically active nanostructures can be used to control light conversion.[27−31] For instance, liquid-crystalline matrixes allow for the tuning of the dielectric environment around noble-metal nanostructures as the light-induced isotropic-to-nematic phase transition occurs.[32,33] Azobenzene-based materials can also be used as an active medium with a changeable refractive index for noble-metal nanostructures.[34−36] The photoswitching of the LSPR of gold and silver nanostructures was recently demonstrated using self-assembled monolayers (SAMs) deposited on gold nanostructures.[37,38] In particular, an extremely small LSPR shift of 0.04 nm was observed upon the trans−cis photoisomerization of simple azobenzenes with a propylene spacer.[39] Another report showed that an azobenzene SAM on gold nanoprisms induced up to a 21-nm LSPR shift upon trans−cis isomerization of the SAM.[40] It should be noted that both reports utilized gold nanostructures with an LSPR far from the $\pi-\pi^*$ and $n-\pi^*$ absorption bands of azobenzenes. Furthermore, SAM-based systems are often unpredictable and can depend strongly on monolayer packing and preparation conditions.[41] In photochromic materials, the change in refractive index stems from the change in electronic distribution and, hence, the molecular polarizability.[42]

Some reports have clearly demonstrated that the refractive index variation during photoisomerization is highest near the absorption wavelength of a photochromic material. For instance, Nishi et al. employed photochromic diarylethene polymer coatings of gold nanoparticles to induce changes in LSPR peak position and magnitude.[43] Baudrion et al. used a spiropyran molecule in its monomeric form to create a variable-refractive-index medium.[44] By varying the diameter of the nanoparticles, they were able to achieve strong coupling between the surface plasmon and the excited state of an organic molecule, resulting in a large plasmonic response. Finally, our group recently established reversible LSPR switching using electrochromic polymers driven by a substantial refractive index change that accompanied a colored-to-transmissive transition.[13] Despite significant progress, issues in achieving stable and reproducible plasmonic modulation remain. For instance, the use of electrochromic active matrixes requires metal structures with high oxidative stability, and many photochromic systems lack chemical and thermal stability.[45,46]

Here, we report on the fabrication of light-responsive silver nanocube arrays embedded in a photoactive medium based on newly synthesized branched azobenzene-modified polyhedral oligomeric silsesquioxanes (POSS), Azo-POSS, that are able to form uniform, stable, ultrathin films and have an absorption peak overlapping with the LSPR of silver nanocubes (Figure 1). This design induces LSPR modulation through the high refractive index change of azobenzene in its trans and cis states in the wavelength range of 350−500 nm that is easily measurable with conventional spectrophotometers.

Furthermore, we investigated the properties of these hybrid materials in search of an optimal molecular structure with the highest photoinitiated changes. We found that the Azo-POSS branched conjugate with a short spacer between the core and the dye branches has a larger refractive index variation than azobenzene dye embedded in a poly(methyl methacrylate) (PMMA) matrix. Most importantly, we observed a stable and reversible LSPR switching upon alternating irradiation of the coating with UV and visible light. The experimental results are supported by finite-difference time-domain (FDTD) simulations. Finally, the observation of reflectance in total-internal-reflection (TIR) experiments under polarized light revealed the polarization-dependent LSPR modulation of embedded nanocubes. We suggest that the design of an active plasmonic array reported here can be further extended to include azobenzene analogues covering the entire visible spectrum for applications in stable, tunable optical materials.

EXPERIMENTAL SECTION

Compounds **1** and **2** were prepared using a hydrosilylation approach with POSS-H as a scaffold for the attachment of azo dyes bearing reactive allyloxy groups. Compounds **AB** and **2** were reported previously;[47] synthesis of compound **1** is described in the Supporting Information (see Scheme S1).

The UV−vis spectra were recorded on a Shimadzu UV-2450 spectrophotometer with a spectral resolution of 0.5 nm for the UV/vis cycling experiment and 1 nm for other measurements. Peak picking was performed using the OriginLab Origin 8.5 built-in peak analyzer tool (20-point local maximum). Photoisomerization experiments were performed by irradiating the samples at a 10-cm distance with 365-nm unpolarized UV light from a Blak-Ray model B-100A UV lamp (100 W) and then recording the absorbance spectra. Visible light irradiation for the reverse isomerization was conducted with unpolarized light from a 26-W compact fluorescent lamp. For kinetics measurements, the quartz cuvette containing the sample was irradiated with 365-nm

DOI: 10.1021/am508993z
ACS Appl. Mater. Interfaces 2015, 7, 4902−4912

Scheme 1. Azo-POSS Conjugates Used in This Study

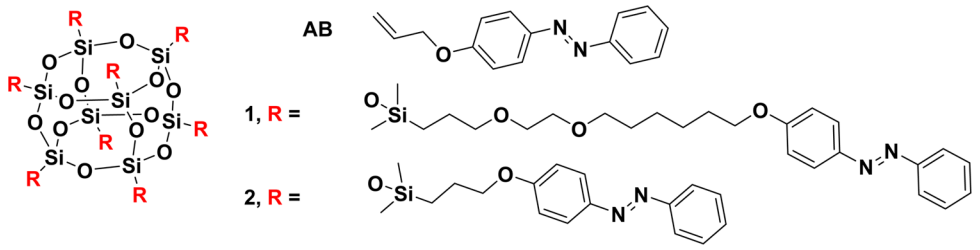

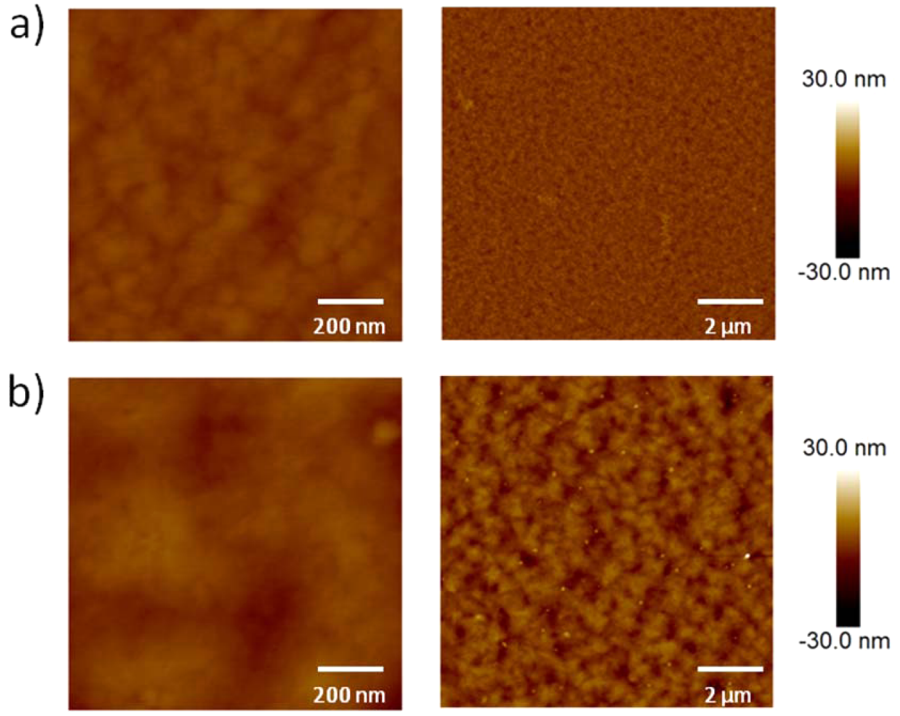

Figure 2. AFM topographical images of ultrathin films prepared by spin-casting (a) compound **1** and (b) compound **2** onto silicon substrates at different magnifications.

UV light, and the absorption spectrum was recorded every 10 s. The experiment was performed in triplicate.

Spin-coating was performed by dropping the solution of compound **1** or **2** in toluene (2 wt %) onto a silicon or quartz substrate and rotating the sample for 30 s at 3000 rpm on a spin-coater (Laurell). The solutions were filtered through a filter with a mesh size of 200 nm before spin-coating, and the films were dried in ambient conditions before measurements. The AB-PMMA thin films where the dye was not tethered to a POSS core were prepared by spin-coating from an 8 wt % solution of AB-PMMA (3:5, w/w) in anisole under the same conditions. The resulting film had a thickness of 210 nm as determined by spectroscopic ellipsometry.

Spectroscopic ellipsometry was performed on a M-2000U ellipsometer (Woollam). The spectral range was 245−1000 nm (D2 and QTH lamps). Ellipsometry data from all samples were acquired at 65°, 70°, and 75° angles of incidence over the spectral range. The Azo-POSS layers were fit with a three-layer model consisting of a silicon substrate, a silicon oxide layer (2-nm layer thickness), and a Cauchy layer [mean squared error (MSE) < 4] in the range from 550 to 1000 nm. The complex refractive index was then determined by point-by-point fitting over the entire spectral range. This reference function was used in the general oscillator layer to obtain dispersion curves by fitting with Gaussian functions.

Atomic force microscopy (AFM) scanning of the thin films was conducted using a Dimension 3000 microscope (Digital Instruments) in tapping mode. Scans were performed at a rate of 0.5−1.0 Hz for surface areas of 1 × 1 μm^2, 5 × 5 μm^2, and 10 × 10 μm^2 according to the usual procedure employed in our laboratory.[48] Silicon nitride AFM tips (MikroMasch) with a spring constant of 7 N/m and a resonant frequency of ca. 150 kHz were used for AFM imaging. The AFM images were collected at a resolution of 512 × 512 pixels.

Total-internal-reflection (TIR) measurements for the silver nanocube films were conducted with the spectroscopic ellipsometer in reflection mode over a wavelength range of 300−1000 nm using both s- and p-polarized light at an incident angle of 50° with a spectral resolution of 1.59 nm. The spectra were smoothed using a seven-point fast Fourier transform (FFT) filter (OriginLab Origin 8.5). For total internal reflection, we employed a CaF_2 prism (25-mm base, right angle, uncoated, from Thorlabs). A single drop of diethylene glycol was applied to the bottom of the prism as immersion oil where the opposite (uncoated) side of the nanocube and Azo-POSS-covered quartz slide made contact. Care was taken with proper coverage of immersion oil to ensure that no air gaps occurred at the prism−slide interface. The prism−oil−slide setup was mounted on the ellipsometer stage with the silver nanocube coating facing down, making no contact with the stage. As a control, an uncoated quartz slide was measured for every polarization measurement.

Finite-difference time-domain (FDTD) simulations were conducted using commercial software from Lumerical Solutions (FDTD Solutions 8.7.4). Nine nanocubes were modeled in a "square" configuration with a 50-nm edge length, 25% edge rounding, and a 127-nm interparticle distance based on transmission electron microscopy (TEM) and scanning electron microscopy (SEM) analysis of a typical sample. The average nanocube edge length and edge

DOI: 10.1021/am508993z
ACS Appl. Mater. Interfaces 2015, 7, 4902−4912

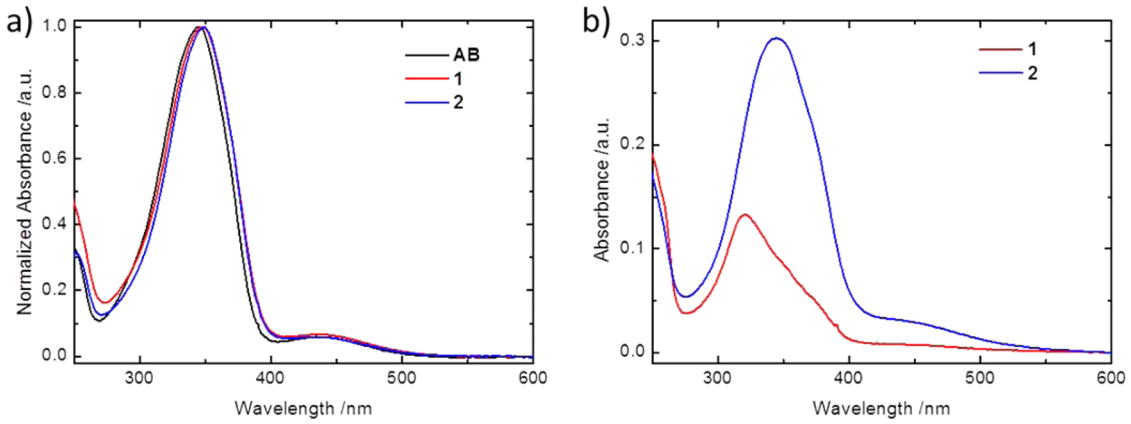

Figure 3. UV−vis absorbance spectra of (a) compounds **AB**, **1**, and **2** in $CHCl_3$ (0.01 mg/mL) and (b) compounds **1** and **2** in thin films (thicknesses of 68 and 60 nm, respectively).

rounding were determined using ImageJ software (Figure S1, Supporting Information). The interparticle distance was calculated using the commercial SPIP image processing software. Multiple nanocubes were modeled to take into account interparticle coupling between nanocubes and the resulting changes in their optical behavior. Nanocubes were also modeled with a 2-nm poly(vinylpyrrolidone) (PVP) coating, as determined in our previous studies.[13] An 80-nm POSS layer was added using refractive index values imported from ellipsometry measurements for both the trans and cis isomers. Silver nanocube dielectric values were obtained from the built-in CRC material data.[49] Perfectly matched layer (PML) boundaries were used in simulations to prevent interior reflection at the boundaries. A total-field scattered-field plane-wave light source with a wavelength range of 300−1000 nm was used for excitation. Last, a 2-nm mesh was used across the entire simulation region in all directions.

RESULTS AND DISCUSSION

Azobenzene-Based Hybrid Materials. Conjugation of azobenzenes to POSS results in hybrid materials with high thermal and photostability that are compatible with organic solvents for solution processing.[50−52] Indeed, it has been found that it is possible to obtain stable ultrathin films from Azo-POSS conjugates.[53,47] Importantly, the reversible photoisomerization of azobenzene still occurs in such stable Azo-POSS films, enabling their applications in photoresponsive systems. The azobenzene conjugates, such as 4-phenylazophenol derivatives, have a relatively high energy barrier for cis-to-trans thermal relaxation, with cis isomer lifetimes on the order of days. This behavior can facilitate the examination of the material in different states. The rate of trans-to-cis photoisomerization of azobenzene in solution was found to depend only slightly on grafting to the POSS core.[50,51] To elucidate the role of azobenzene conjugation, we utilized two AZO-POSS compounds, **1** and **2**, with different spacer lengths between the inorganic core and the azobenzene moiety (Scheme 1). As is known, the linker length (4 versus 10 methylene units) has a pronounced effect on thermal cis-to-trans relaxation.[52] Therefore, we synthesized two compounds: compound **1** with a linker length between a Si atom of the POSS moiety and a benzene ring of 1.87 nm when fully extended and compound **2** with a linker length of 0.7 nm (estimated from Chem3D modeling). Furthermore, we employed a precursor azobenzene compound **AB** for comparison with Azo-POSS conjugates (Scheme 1).

Ultrathin Films from Azo-POSS Compounds. Ultrathin films of compounds **1** and **2** can be spin-cast onto flat substrates from solutions in toluene or chloroform. A 2 wt % solution of compound **1** or **2** in toluene formed uniform films of 68 or 60 nm, respectively, when spin-cast at 3000 rpm (Figure 2).

Surface analysis using AFM revealed that compound **1** yielded a smooth film with a root-mean-square (RMS) roughness (Rq) of 1.3 nm (in a 10 μm × 10 μm selected surface area). Compound **2** under the same conditions gave a somewhat less uniform film with an increased microroughness of 5.5 nm (Figure 2b).

Although the UV−vis spectra of compounds **AB**, **1**, and **2** in chloroform solutions are very similar, thin-film absorption spectra reveal a striking difference between compounds **1** and **2** (Figure 3a,b). The absorbance of compound **1** is weaker and blue-shifted (320 nm) compared to that of compound **2** despite the similar film thicknesses. Because of the sensitivity of the $\pi-\pi^*$ transition of azo dyes to aggregation, the hypsochromic shift might indicate the face-to-face stacking of planar *trans*-azobenzene moieties and formation of H-aggregates.[54] We suggest that the longer spacer between the POSS core and azobenzenes of compound **1** allows for more rotational freedom and, consequently, leads to favorable packing of the azobenzene moieties. The ability of POSS-containing compounds **1** and **2** to form ultrathin films makes it possible to accurately determine the refractive indexes of the trans and cis isomers of these compounds for use as a photoactive layer.

Refractive Index Variation. We first investigated the photoswitching behavior of compounds **1** and **2** in 0.01 mg/mL chloroform solutions by monitoring the decay of the $\pi-\pi^*$ transition of *trans*-azobenzene at 350 nm. The first-order rate constant of photoisomerization can be determined from the slope of a plot of $\ln[(A_0 - A_\infty)/(A_t - A_\infty)]$ versus time, where A_0, A_∞, and A_t are the absorbances before irradiation, after reaching a photostationary state, and at a given time t, respectively.[55] The photoisomerization experiment was performed in triplicate for each sample, and the averaged data points and linear fits are presented in Figure S3c (Supporting Information). We found that compounds **1** and **2** had similar photoisomerization rates in chloroform solution: 0.192 ± 0.054 and 0.186 ± 0.029 s^{-1}, respectively (Figure S3, Supporting Information).[47]

This difference indicates that the spacer length between the POSS core and the azobenzene moiety of compound **2** is already sufficient for unrestricted photoisomerization of the azobenzene arms in solution. A further increase in linker length

DOI: 10.1021/am508993z
ACS Appl. Mater. Interfaces 2015, 7, 4902−4912

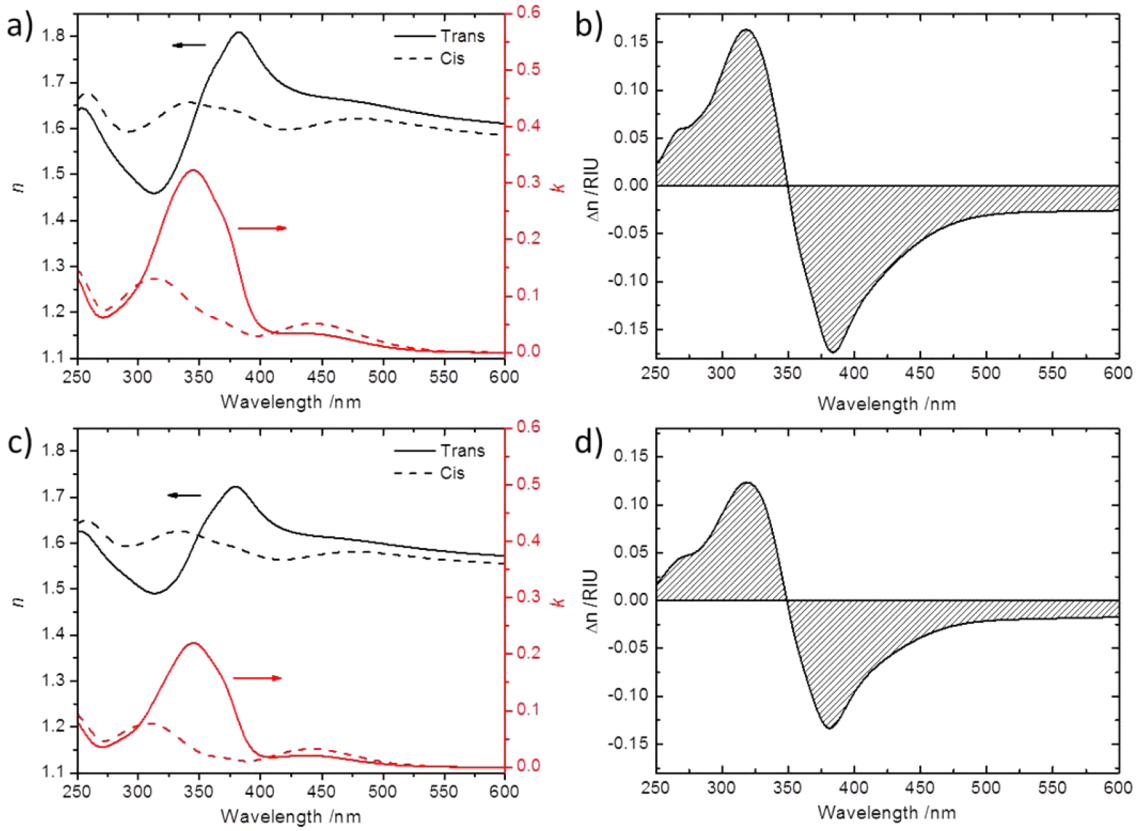

Figure 4. (a) Dispersion curves for thin films of compound **2** in trans and cis forms. (b) Refractive index difference between the trans and cis forms in a thin film of compound **2**. (c) Dispersion curves for thin films of AB-PMMA in trans and cis forms. (d) Refractive index difference between the trans and cis forms in a thin film of AB-PMMA.

in compound **1**, therefore, has only a small effect on the rate of photoisomerization in solution. In contrast, when the film of compound **1** was irradiated with an unpolarized 365-nm UV light, virtually no change in absorbance was observed. The thin film of compound **2**, however, exhibited a pronounced change in intensity of the $\pi-\pi^*$ transition at 350 nm, indicating efficient trans-to-cis isomerization (Figure S3e, Supporting Information).[47] We therefore focused on compound **2** as a variable-refractive-index medium for subsequent studies.

A study of film morphology during photoisomerization showed that the as-spun film of compound **2** had a roughened surface with crystalline domains clearly visible in an AFM phase image (Figure S4a, Supporting Information). However, after UV irradiation, the film surface became extremely smooth without any visible phase contrast (Figure S4b, Supporting Information). This observation can be explained by the tendency of linear-shaped *trans*-azobenzene to crystallize and the nonplanar cis isomer to have less favorable packing, resulting in a smooth thin film. The thin film of **2** returned to its initial roughened state after cis-to-trans thermal relaxation in the dark for several days. However, the cis–trans photoisomerization upon alternating UV/vis irradiation did not affect the thin-film morphology (Figure S4c, Supporting Information). To exclude the effect of film morphology, all subsequent experiments were conducted after the ultrathin film of compound **2** was subjected to one UV/vis irradiation cycle. Also, the overall thickness of azobenzene-containing thin films was reported to change on the order of 1–2% in some cases.[56] In our experiments, we observed that the thickness of films of **2** determined by spectroscopic ellipsometry did not change upon photoisomerization.

To compare the performance of the Azo-POSS material to azobenzene-doped polymer films, we considered films in which a poly(methyl methacrylate) PMMA matrix was mixed with the precursor compound **AB** in the highest possible ratio of 3:5 (henceforth AB-PMMA). We used thin films of compound **2** and AB-PMMA to obtain the real part of the complex refractive index. In a typical experiment, the sample was irradiated for 5 min at 365 nm to achieve trans-to-cis photoisomerization and then for 5 min with white light for reverse isomerization. The refractive indices of the composites were obtained by fitting the reference data for the imaginary part of the refractive index with five (cis form) or six (trans form) Gaussian oscillators followed by a Kramers–Kronig transformation (Figure 4).

Analysis of the dispersion curves revealed that a significant change in refractive index occurred in the spectral window from 250 to 500 nm for compound **2** and AB-PMMA films. The refractive index difference (Δn) between the trans and cis forms of azobenzene-containing materials is defined as $\Delta n(\lambda) = n_{cis}(\lambda) - n_{trans}(\lambda)$. The largest change was found to occur at 380 nm and equaled −0.17 refractive index units (RIU) for compound **2** and −0.13 RIU for the AB-PMMA film upon trans-to-cis isomerization. These values compare favorably with the literature data for other chromic compounds.[26,44,57] The photochromic spiropyran has the highest refractive index variation at approximately 500 nm (−0.06 RIU) and 610 nm (from +0.16 to +0.19 RIU depending on the dye doping level). The electrochromic bistable rotaxane system provides a change of +0.011 RIU at 690 nm and −0.017 RIU at 970 nm.

DOI: 10.1021/am508993z
ACS Appl. Mater. Interfaces 2015, 7, 4902–4912

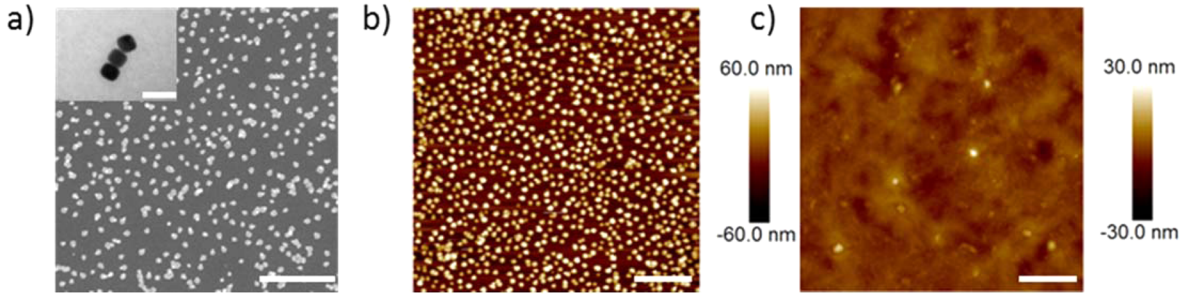

Figure 5. (a) SEM image of silver nanocubes on a silicon substrate prepared by LB deposition. The inset shows a TEM image of silver nanocubes (scale bar is 100 nm). (b,c) AFM topographical images (5×5 μm^2) of (b) silver nanocubes on a quartz slide deposited by LB deposition and (c) composite material composed of a silver nanocube monolayer covered with compound **2**. The scale bar is 1 μm for all images.

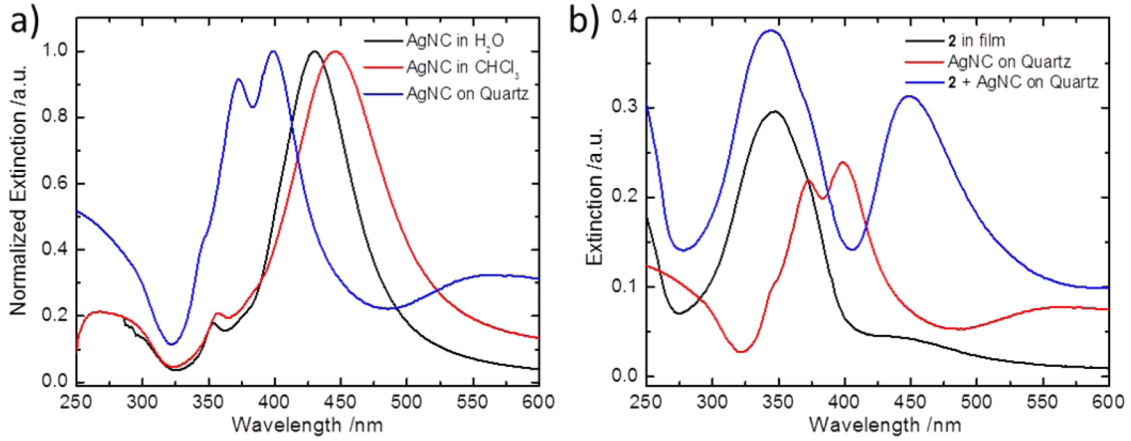

Figure 6. UV−vis spectra of (a) silver nanocubes (AgNC) in H_2O and $CHCl_3$ and after deposition on quartz and (b) a silver nanocube monolayer on quartz coated with a thin layer of compound **2**. In b, spectra of compound **2** and silver nanocubes on quartz are provided for reference.

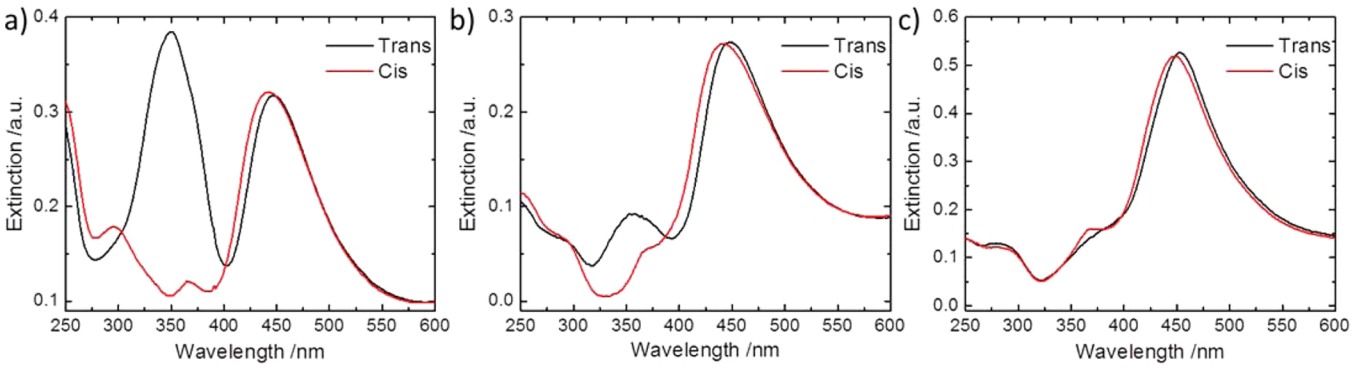

Figure 7. UV−vis spectra of (a) silver nanocubes coated with compound **2** after UV irradiation (cis) and visible light irradiation (trans), (b) silver nanocubes coated with compound **2** after UV irradiation (cis) and visible light irradiation (trans) normalized to the corresponding spectra of the compound **2** film, and (c) silver nanocubes coated with an AB-PMMA layer after UV irradiation (cis) and visible light irradiation (trans) normalized to the corresponding spectra of the AB-PMMA layer.

Therefore, the Azo-POSS photochromes investigated in this study complement the existing active matrixes in the 350−500 nm spectral window where the plasmon resonances of individual silver nanocubes are located. The larger refractive index variation for compound **2** compared to AB-PMMA can be explained by a higher functional group density. Indeed, compound **2** has a POSS core-to-azo dye ratio of 1:1.7, whereas AB-PMMA has a ratio of 1:0.6 (as determined by solution concentration). The extinction coefficients measured in thin films, however, are similar: 0.32 for compound **2** compared to 0.22 for AB-PMMA film. It should be noted that an azobenzene-to-polymer weight ratio higher than 3:5 resulted in phase separation in AB-PMMA films. Because of the higher photoinduced refractive index variation of Azo-POSS compound **2** compared to the AB-PMMA, the Azo-POSS compound is promising as an active medium to induce the variation in plasmon resonances of noble-metal nanoparticles in response to UV irradiation of a photoswitchable matrix.

Silver Nanocube-(Azo-POSS) Ultrathin Coatings. Silver nanocubes with a 50-nm edge length were transferred onto precleaned quartz and silicon substrates using the Langmuir−Blodgett (LB) technique and formed densely packed monolayers (Figure 5a,b).[58,59] The relatively low surface pressure during monolayer transfer resulted in well-separated

DOI: 10.1021/am508993z
ACS Appl. Mater. Interfaces 2015, 7, 4902−4912

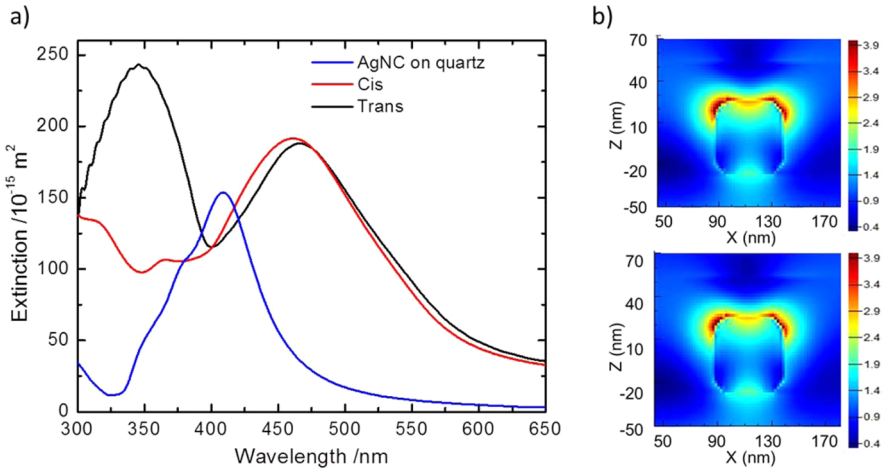

Figure 8. (a) Simulated spectra of silver nanocubes (AgNC) on quartz coated with compound 2 after UV irradiation (cis) and visible light irradiation (trans). (b) Simulated electric field intensity distribution for an individual nanocube embedded in compound **2** in trans (top) and cis (bottom) states. The scale bars are in units of E/E_0.

silver nanocubes with minimal aggregation. The average interparticle distance was estimated to be 127 ± 30 nm based on SEM image analysis.

Next, a solution of compound **2** in toluene (2 wt %) was directly spin-cast on top of the LB monolayer at 3000 rpm. Using AFM cross-section analysis, we established that the total thickness of the composite was 80 nm (Figure S5, Supporting Information). The Rq value of the film was 2.7 nm, which is similar to that of the ultrathin film of Azo-POSS. Compound **2** covered all surfaces of the silver nanocubes completely for maximum exposure to active material (Figure 5c).

The extinction spectra of the silver nanocubes are presented in Figure 6a. The LSPR position is located at 430 nm in water and shifts to 446 nm after the transfer to chloroform (see the Experimental Section). This change is due to the higher refractive index of chloroform (n_{500} = 1.449) compared to water (n_{500} = 1.335) and possibly minor cube-edge rounding during the solvent-exchange procedure. Upon the LB deposition of the nanocube monolayer onto the quartz substrate, the LSPR peak splits into antibonding (373 nm) and bonding (398 nm) modes because of the high refractive index of the quartz substrate (n = 1.46 at a wavelength of 400 nm).[60]

After deposition of a high-index material (compound **2**) on top of and around the silver nanocube monolayer, the LSPR position red-shifted to 445 nm, and the peak splitting disappeared because of the similar refractive indices of the substrate and the active composite layer (Figure 6b). Despite the LSPR of the composite material being shifted from the wavelength of maximum refractive index variation (380 nm), the −0.06 refractive index unit (RIU) change at 445 nm should lead to a significant LSPR modulation, as discussed below.

Photoinduced LSPR Shifting. Silver nanocubes coated with compound **2** showed a 4-nm hypsochromic shift of the LSPR peak from 443 nm when the surrounding Azo-POSS was irradiated with 365-nm light (Figure 7a). Upon exposure to visible light (>450 nm), the LSPR peak returned to its initial position, demonstrating the reversibility of the photoinitiated process. To eliminate the overlap from the changing azobenzene absorption, the corresponding spectra of the film of compound **2** were subtracted from those of the coated nanocube monolayer, thus increasing the apparent shift to 6 nm (Figure 7b).

The LSPR shift can be explained based on exact measurements of the change in refractive index (Δn) upon photoisomerization of compound **2** and the refractive index sensitivity of silver nanocubes. The refractive index change of compound **2** at a particular wavelength can be found from Figure 4a and equals 0.06 RIU at 445 nm (LSPR wavelength). The refractive index sensitivity (RIS = $\Delta\lambda_{LSPR}/\Delta n$) is a measure of the change in plasmonic wavelength in response to the refractive index of the surrounding medium. The RIS depends on multiple factors such as the nanoparticle material and shape, nature of the substrate, size, edge rounding, and interparticle distance.[61,62] Furthermore, the change in LSPR wavelength of silver nanocubes has a linear dependence on the refractive index: a decrease in the surrounding refractive index results in a reduction of the LSPR wavelength (blue shift).[63] The refractive index sensitivity of 65-nm silver nanocubes on a quartz substrate was previously found to be 113 nm/RIU.[64]

Considering the above results, a 6.8-nm hypsochromic LSPR shift can be expected for the combination of materials components, which is close to the experimentally observed LSPR peak shift of 6 nm. The same sequence of estimations can be repeated for a silver nanocube array coated with AB-PMMA layer as an alternative variable-refractive-index material. In this case, because of the smaller change in refractive index of the dye−polymer material (−0.05 RIU at 445 nm), a lower LSPR shift should be and was observed (5 nm) than for the composite layer based upon compound **2** (Figure 7c). Therefore, the higher photoinduced refractive index variation of branched compound **2** with a weight fraction of grafted azobenzene arms and the ease of the robust ultrathin coating fabrication make such hybrid materials promising for applications in photoresponsive plasmonic coatings.

The experimental findings were further confirmed by FDTD simulations (Figure 8a). Silver nanocubes were modeled with a 50-nm edge length and 25% edge rounding based on TEM analysis (see the Experimental Section). A blue shift of 6 nm was observed in the LSPR peak due to refractive index changes of the surrounding material as a result of trans−cis isomerization. It should be noted that the simulated nanocube extinction peak was red-shifted by 20 nm from the experimental findings, most likely because of the monodispersity and perfect periodicity of the FDTD model.

DOI: 10.1021/am508993z
ACS Appl. Mater. Interfaces 2015, 7, 4902−4912

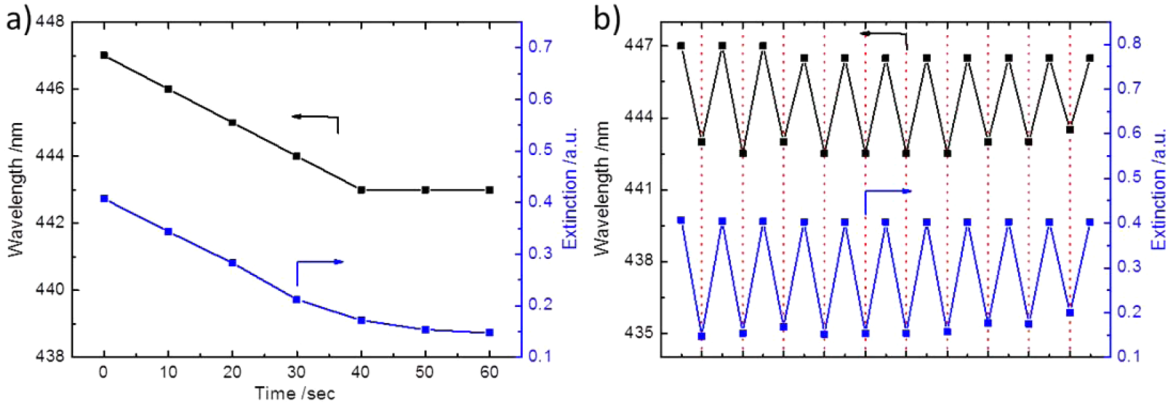

Figure 9. (a) Photoinitiated switching behavior of silver nanocubes coated with Azo-POSS compound **2**. The upper curve is the LSPR position, whereas the bottom curve is the Azo-POSS absorbance at 350 nm. (b) LSPR peak position modulation upon exposure to 365-nm UV light over 10 UV/vis cycles. The dotted lines correspond to UV light exposure.

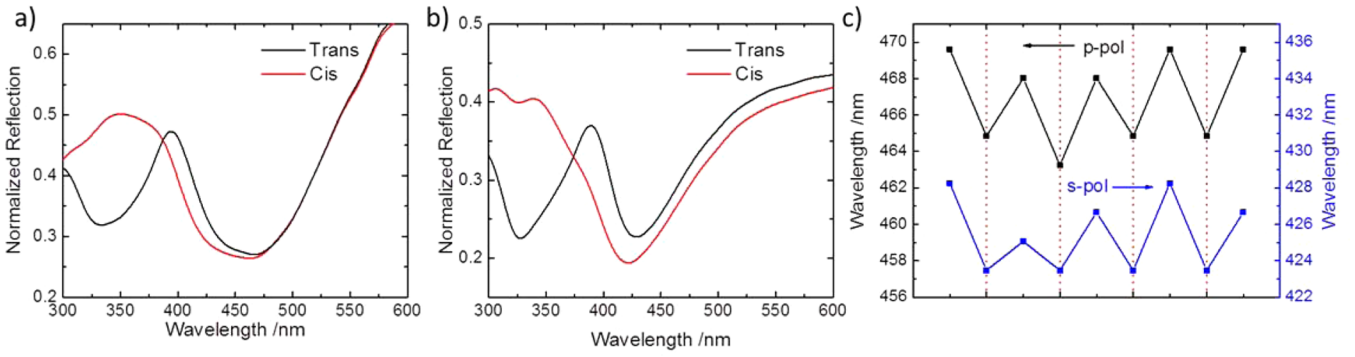

Figure 10. (a,b) TIR measurements of different photoisomerized states with (a) p- and (b) s-polarized light. (c) Switching behavior of the reflectance minimum under alternating irradiation with UV and visible light. The dotted lines correspond to UV irradiation events.

The electric field intensity distributions of the nanocubes embedded in compound **2** for the trans and cis states exhibit relatively minor differences (Figure 8b). Although the plasmonic modes are oriented away from the substrate and would typically be classified as antibonding modes, it should be noted that the direction of light propagation (from the bottom through the quartz substrate) causes this effect and that the observed modes are, in fact, bonding modes.[65,66]

Next, we investigated the control over the LSPR modulation and cycling stability of ultrathin silver nanocube−Azo-POSS films. A plot of LSPR wavelength versus irradiation time is presented in Figure 9a. These data show that fine control of the ratio of trans and cis isomers in the ultrathin film of compound **2** can be achieved by varying the irradiation time. The upper curve is the LSPR position of silver nanocubes, and the bottom curve is the extinction at 350 nm of the Azo-POSS matrix ($\pi-\pi^*$ transition of *trans*-azobenzene). It can be seen that the LSPR modulation follows the change in the trans-isomer fraction in the film of compound **2**. Therefore, it is possible to control the exact LSPR shift by changing the UV exposure time.

A stable switching of compound **2** is illustrated by the highly repeatable reduction and recovery of the *trans*-azobenzene absorption. Reproducible silver nanocube LSPR modulation was observed between 443 and 447 nm as the sample was alternately irradiated with UV and visible light (Figure 9b). The corresponding transmission spectra are provided in Figure S6 (Supporting Information). The average plasmon resonance shift over 10 cycles was 3.8 ± 0.4 nm, with local deviations within 10%. Such stability arises from a strong adhesion of the LB monolayer of silver nanocubes to the quartz substrate and the photostability of ultrathin coatings of Azo-POSS compound **2**. Topographical images of the composite material obtained after multiple switching cycles show a relatively smooth morphology with an Rq value of 2.4 nm after UV irradiation and 2.5 nm after visible light irradiation (Figure S7, Supporting Information). Azobenzene-containing thin films can form surface relief gratings (SRGs) as a result of photoinduced molecular displacement when in close contact with metallic nanostructures.[65,67] This aspect of the photoresponsive plasmonic system reported here will be investigated in due course.

LSPR Modulations in the Total-Internal-Reflection Regime. The placement of silver nanocubes as a monolayer at the surface of the quartz slide coated with a layer of compound **2** creates an anisotropic environment where the refractive index of the substrate (n_{450} = 1.47) is lower than that of the active matrix (n_{450} = 1.67). We considered that this index mismatch generates symmetry breaking and dipolar mode broadening similar to that observed for the quartz−air interphase (Figure 6). The modes oscillate parallel and perpendicular to the quartz−Azo-POSS interphase and can be distinguished under incident polarized light. Thus, we chose a total-internal-reflection (TIR) setup to probe the refractive index variation of silver nanocube−Azo-POSS ultrathin films by exciting the nanocube LSPR with evanescent waves. As is known, the TIR regime occurs at an angle beyond the critical angle of the quartz−air interface (>43°), known from the

DOI: 10.1021/am508993z
ACS Appl. Mater. Interfaces 2015, 7, 4902−4912

following relation derived from Snell's law: $\theta_c = \sin^{-1}(n_{air}/n_{quartz})$.[68]

Under TIR conditions, a pronounced difference in reflection spectra between s- and p-polarized incident light is observed (Figure 10). There is a noticeable blue shift and line-width narrowing of the LSPR from p-polarized light to s-polarized light. For the trans state, the LSPR is observed at 468 nm under p-polarized (parallel to the plane of incidence) light and at 427 nm under s-polarized (perpendicular to the plane of incidence) light. This difference can be explained by the fact that, at a 50° angle of incidence, p-polarized light excites oscillation both perpendicular and parallel to the interphase whereas s-polarized light excites only the component parallel to the interphase (Figure 10b).[69] The measurement under p-polarized light is therefore more sensitive to the refractive index variation, and the LSPR shifts during photoisomerization were measured at 4.4 ± 0.7 and 3.4 ± 1.3 nm for p- and s-polarized light, respectively, over four cycles (Figure 10 c). As with transmission extinction measurements, we observed a reversible cycling of reflection in the TIR regime when the sample was alternately irradiated with UV and visible light.

CONCLUSIONS

In conclusion, we have reported the fabrication of responsive silver nanocube arrays embedded in an active medium based on newly synthesized branched Azo-POSS compounds. The branched conjugate with a long spacer between the core and the azobenzene branches undergoes photoisomerization in solution but not in an ultrathin solid film. Azo-POSS conjugate **2**, with a shorter spacer between the core and the azobenzene moieties, exhibits a large refractive index variation when irradiated with UV light (−0.17 RIU change at a wavelength of 380 nm), higher than that of simple azobenzene embedded in a polymer matrix. We observed significant, reversible, and repeatable shifts in silver nanocube LSPR peak position (from 4 to 6 nm) upon alternating irradiation of the composite Azo-POSS−nanocube ultrathin film with UV and visible light. Furthermore, a polarization-dependent variation in reflectance was observed in the TIR regime, supporting the ability to reversibly tune the LSPR by external stimuli such as light. Although the plasmonic response of the hybrid material based on mono azobenzene reported here is relatively slow (on the order of minutes), the use of push−pull azobenzenes with faster photoisomerization kinetics in a similar setup can shorten the response time and shift the operational wavelength into the visible wavelength range. Such robust photoswitchable plasmonic materials could find application in plasmonic devices with real-time and polarization-dependent responses, which have the potential for optical switching and filtering applications. In future research, the polarization-dependent behavior of azobenzene-containing materials can be combined with nanoparticle arrays to probe the photoinduced anisotropy of the photoactive materials. Furthermore, oriented anisotropic nanostructures combined with such active layers could result in active polarizers and other devices.

ASSOCIATED CONTENT

Supporting Information

Experimental procedures, NMR and FTIR spectra of compound **1**, Figures S1−S7. This material is available free of charge via the Internet at http://pubs.acs.org.

AUTHOR INFORMATION

Corresponding Author

*E-mail: vladimir@mse.gatech.edu.

Notes

The authors declare no competing financial interest.

ACKNOWLEDGMENTS

We thank Dr. Tobias König (University of Bayreuth, Bayreuth, Germany) for useful discussions. We thank Weinan Xu and Ren Geryak for assistance with the TEM measurements and statistical analysis of the silver nanocubes. This work was supported by the National Science Foundation, Grant NSF-DMR 1002810 (Synthesis of Branched Compounds and Film Morphology), and the Department of Energy, Office of Basic Energy Sciences, Division of Materials Sciences and Engineering, under Award DE-FG02-09ER46604 (Synthesis of Nanocubes, Optical Properties, Simulations, and Photoisomerization).

REFERENCES

(1) Ferry, V. E.; Munday, J. N.; Atwater, H. A. Design Considerations for Plasmonic Photovoltaics. *Adv. Mater.* **2010**, *22*, 4794−4808.
(2) Gan, Q. Q.; Bartoli, F. J.; Kafafi, Z. H. Plasmonic-Enhanced Organic Photovoltaics: Breaking the 10% Efficiency Barrier. *Adv. Mater.* **2013**, *25*, 2385−2396.
(3) Lang, X.; Chen, X.; Zhao, J. Heterogeneous Visible Lght Photocatalysis for Selective Organic Transformations. *Chem. Soc. Rev.* **2014**, *43*, 473−486.
(4) Sau, T. K.; Rogach, A. L.; Jackel, F.; Klar, T. A.; Feldmann, J. Properties and Applications of Colloidal Nonspherical Noble Metal Nanoparticles. *Adv. Mater.* **2010**, *22*, 1805−1825.
(5) Saha, K.; Agasti, S. S.; Kim, C.; Li, X. N.; Rotello, V. M. Gold Nanoparticles in Chemical and Biological Sensing. *Chem. Rev.* **2012**, *112*, 2739−2779.
(6) Ozbay, E. Plasmonics: Merging Photonics and Electronics at Nanoscale Dimensions. *Science* **2006**, *311*, 189−193.
(7) Gramotnev, D. K.; Bozhevolnyi, S. I. Plasmonics Beyond the Diffraction Limit. *Nat. Photonics* **2010**, *4*, 83−91.
(8) Murray, W. A.; Barnes, W. L. Plasmonic Materials. *Adv. Mater.* **2007**, *19*, 3771−3782.
(9) Gupta, M. K.; König, T.; Near, R.; Nepal, D.; Drummy, L. F.; Biswas, S.; Naik, S.; Vaia, R. A.; El-Sayed, M. A.; Tsukruk, V. V. Surface Assembly and Plasmonic Properties in Strongly Coupled Segmented Gold Nanorods. *Small* **2013**, *9*, 2979−2990.
(10) Cialla, D.; Marz, A.; Bohme, R.; Theil, F.; Weber, K.; Schmitt, M.; Popp, J. Surface-Enhanced Raman Spectroscopy (SERS): Progress and Trends. *Anal. Bioanal. Chem.* **2012**, *403*, 27−54.
(11) Boriskina, S. V.; Ghasemi, H.; Chen, G. Plasmonic Materials for Energy: From Physics to Applications. *Mater. Today* **2013**, *16*, 375−386.
(12) Combs, Z. A.; Malak, S. T.; König, T.; Mahmoud, M. A.; Chavez, J. L.; El-Sayed, M. A.; Kelley-Loughnane, N.; Tsukruk, V. V. Aptamer-Assisted Assembly of Gold Nanoframe Dimers. *Part. Part. Syst. Charact.* **2013**, *30*, 1071−1078.
(13) König, T. A. F.; Ledin, P. A.; Kerszulis, J.; Mahmoud, M. A.; El-Sayed, M. A.; Reynolds, J. R.; Tsukruk, V. V. Electrically Tunable Plasmonic Behavior of Nanocube-Polymer Nanomaterials Induced by a Redox-Active Electrochromic Polymer. *ACS Nano* **2014**, *8*, 6182−6192.
(14) Stuart, M. A.; Huck, W. T.; Genzer, J.; Muller, M.; Ober, C.; Stamm, M.; Sukhorukov, G. B.; Szleifer, I.; Tsukruk, V. V.; Urban, M.; Winnik, F.; Zauscher, S.; Luzinov, I.; Minko, S. Emerging Applications of Stimuli-Responsive Polymer Materials. *Nat. Mater.* **2010**, *9*, 101−113.

DOI: 10.1021/am508993z
ACS Appl. Mater. Interfaces 2015, 7, 4902−4912

(15) Karg, M.; Pastoriza-Santos, I.; Perez-Juste, J.; Hellweg, T.; Liz-Marzan, L. M. Nanorod-Coated PNIPAM Microgels: Thermoresponsive Optical Properties. *Small* **2007**, *3*, 1222−1229.
(16) Karg, M.; Lu, Y.; Carbo-Argibay, E.; Pastoriza-Santos, I.; Perez-Juste, J.; Liz-Marzan, L. M.; Hellweg, T. Multiresponsive Hybrid Colloids Based on Gold Nanorods and Poly(NIPAM-*co*-allylacetic acid) Microgels: Temperature- and pH-Tunable Plasmon Resonance. *Langmuir* **2009**, *25*, 3163−3167.
(17) Sanchez-Iglesias, A.; Grzelczak, M.; Rodriguez-Gonzalez, B.; Guardia-Giros, P.; Pastoriza-Santos, I.; Perez-Juste, J.; Prato, M.; Liz-Marzan, L. M. Synthesis of Multifunctional Composite Microgels via in Situ Ni Growth on pNIPAM-Coated Au Nanoparticles. *ACS Nano* **2009**, *3*, 3184−3190.
(18) Gupta, S.; Agrawal, M.; Uhlmann, P.; Simon, F.; Stamm, M. Poly(*N*-isopropyl acrylamide)−Gold Nanoassemblies on Macroscopic Surfaces: Fabrication, Characterization, and Application. *Chem. Mater.* **2010**, *22*, 504−509.
(19) Lu, Y.; Mei, Y.; Drechsler, M.; Ballauff, M. Thermosensitive Core−Shell Particles as Carriers for Ag Nanoparticles: Modulating the Catalytic Activity by a Phase Transition in Networks. *Angew. Chem., Int. Ed.* **2006**, *45*, 813−816.
(20) Gehan, H.; Mangeney, C.; Aubard, J.; Levi, G.; Hohenau, A.; Krenn, J. R.; Lacaze, E.; Felidj, N. Design and Optical Properties of Active Polymer-Coated Plasmonic Nanostructures. *J. Phys. Chem. Lett.* **2011**, *2*, 926−931.
(21) Tokareva, I.; Minko, S.; Fendler, J. H.; Hutter, E. Nanosensors Based on Responsive Polymer Brushes and Gold Nanoparticle Enhanced Transmission Surface Plasmon Resonance Spectroscopy. *J. Am. Chem. Soc.* **2004**, *126*, 15950−15951.
(22) Tokarev, I.; Tokareva, I.; Minko, S. Gold-Nanoparticle-Enhanced Plasmonic Effects in a Responsive Polymer Gel. *Adv. Mater.* **2008**, *20*, 2730−2734.
(23) Kozlovskaya, V.; Kharlampieva, E.; Khanal, B. P.; Manna, P.; Zubarev, E. R.; Tsukruk, V. V. Ultrathin Layer-by-Layer Hydrogels with Incorporated Gold Nanorods as pH-Sensitive Optical Materials. *Chem. Mater.* **2008**, *20*, 7474−7485.
(24) Gupta, M. K.; Chang, S.; Singamaneni, S.; Drummy, L. F.; Gunawidjaja, R.; Naik, R. R.; Tsukruk, V. V. pH-triggered SERS via Modulated Plasmonic Coupling in Individual Bimetallic Nanocobs. *Small* **2011**, *7*, 1192−1198.
(25) Stockhausen, V.; Martin, P.; Ghilane, J.; Leroux, Y.; Randriamahazaka, H.; Grand, J.; Felidj, N.; Lacroix, J. C. Giant Plasmon Resonance Shift Using Poly(3,4-ethylenedioxythiophene) Electrochemical Switching. *J. Am. Chem. Soc.* **2010**, *132*, 10224−10226.
(26) Zheng, Y. B.; Yang, Y. W.; Jensen, L.; Fang, L.; Juluri, B. K.; Flood, A. H.; Weiss, P. S.; Stoddart, J. F.; Huang, T. J. Active Molecular Plasmonics: Controlling Plasmon Resonances with Molecular Switches. *Nano Lett.* **2009**, *9*, 819−825.
(27) Rivas, J. G.; Kuttge, M.; Kurz, H.; Bolivar, P. H.; Sanchez-Gil, J. A. Low-Frequency Active Surface Plasmon Optics on Semiconductors. *Appl. Phys. Lett.* **2006**, *88*, 082106−1−082106−3.
(28) Krasavin, A. V.; Zheludev, N. I. Active plasmonics: Controlling Signals in Au/Ga Waveguide Using Nanoscale Structural Transformations. *Appl. Phys. Lett.* **2004**, *84*, 1416−1418.
(29) Andrew, P.; Barnes, W. L. Energy Transfer Across a Metal Film Mediated by Surface Plasmon Polaritons. *Science* **2004**, *306*, 1002−1005.
(30) Bozhevolnyi, S. I.; Volkov, V. S.; Devaux, E.; Laluet, J. Y.; Ebbesen, T. W. Channel Plasmon Subwavelength Waveguide Components Including Interferometers and Ring Resonators. *Nature* **2006**, *440*, 508−511.
(31) Dintinger, J.; Klein, S.; Ebbesen, T. W. Molecule-Surface Plasmon Interactions in Hole Arrays: Enhanced Absorption, Refractive Index Changes, and All-optical Switching. *Adv. Mater.* **2006**, *18*, 1267−1270.
(32) Wang, H.; Vial, A. Plasmonic Resonance Tunability and Surface-Enhanced Raman Scattering Gain of Metallic Nanoparticles Embedded in a Liquid Crystal Cell. *J. Phys. Chem. C* **2013**, *117*, 24537−24542.
(33) Hsiao, V. K. S.; Zheng, Y. B.; Juluri, B. K.; Huang, T. J. Light-Driven Plasmonic Switches Based on Au Nanodisk Arrays and Photoresponsive Liquid Crystals. *Adv. Mater.* **2008**, *20*, 3528−3532.
(34) Xu, S.; Shan, J.; Shi, W.; Liu, L.; Xu, L. Modifying Photoisomerization Efficiency by Metallic Nanostructures. *Opt. Express* **2011**, *19*, 12336−12341.
(35) Tsukruk, V. V.; Luzinov, I.; Larson, K.; Li, S.; McGrath, D. V. Intralayer Reorganization of Photochromic Molecular Films. *J. Mater. Sci. Lett.* **2001**, *20*, 873−876.
(36) Sidorenko, A.; Houphouet-Boigny, C.; Villavicencio, O.; Hashemzadeh, M.; McGrath, D. V.; Tsukruk, V. V. Photoresponsive Langmuir Monolayers from Azobenzene-Containing Dendrons. *Langmuir* **2000**, *16*, 10569−10572.
(37) Manna, A.; Chen, P. L.; Akiyama, H.; Wei, T. X.; Tamada, K.; Knoll, W. Optimized Photoisomerization on Gold Nanoparticles Capped by Unsymmetrical Azobenzene Disulfides. *Chem. Mater.* **2003**, *15*, 20−28.
(38) Ahonen, P.; Schiffrin, D. J.; Paprotny, J.; Kontturi, K. Optical Switching of Coupled Plasmons of Ag-Nanoparticles by Photoisomerisation of an Azobenzene ligand. *Phys. Chem. Chem. Phys.* **2007**, *9*, 651−658.
(39) Muller, M.; Jung, U.; Gusak, V.; Ulrich, S.; Holz, M.; Herges, R.; Langhammer, C.; Magnussen, O. Localized Surface Plasmon Resonance Investigations of Photoswitching in Azobenzene-Functionalized Self-Assembled Monolayers on Au. *Langmuir* **2013**, *29*, 10693−10699.
(40) Joshi, G. K.; Blodgett, K. N.; Muhoberac, B. B.; Johnson, M. A.; Smith, K. A.; Sardar, R. Ultrasensitive Photoreversible Molecular Sensors of Azobenzene-Functionalized Plasmonic Nanoantennas. *Nano Lett.* **2014**, *14*, 532−540.
(41) Evans, S. D.; Johnson, S. R.; Ringsdorf, H.; Williams, L. M.; Wolf, H. Photoswitching of Azobenzene Derivatives Formed on Planar and Colloidal Gold Surfaces. *Langmuir* **1998**, *14*, 6436−6440.
(42) Delaire, J. A.; Nakatani, K. Linear and Nonlinear Optical Properties of Photochromic Molecules and Materials. *Chem. Rev.* **2000**, *100*, 1817−1846.
(43) Nishi, H.; Asahi, T.; Kobatake, S. Light-Controllable Surface Plasmon Resonance Absorption of Gold Nanoparticles Covered with Photochromic Diarylethene Polymers. *J. Phys. Chem. C* **2009**, *113*, 17359−17366.
(44) Baudrion, A. L.; Perron, A.; Veltri, A.; Bouhelier, A.; Adam, P. M.; Bachelot, R. Reversible Strong Coupling in Silver Nanoparticle Arrays Using Photochromic Molecules. *Nano Lett.* **2013**, *13*, 282−286.
(45) Schomburg, C.; Wark, M.; Rohlfing, Y.; Schulz-Ekloff, G.; Wohrle, D. Photochromism of Spiropyran in Molecular Sieve Voids: Effects of Host-Guest Interaction on Isomer Status, Switching Stability and Reversibility. *J. Mater. Chem.* **2001**, *11*, 2014−2021.
(46) Ventura, C.; Thornton, P.; Giordani, S.; Heise, A. Synthesis and Photochemical Properties of Spiropyran Graft and Star Polymers Obtained by 'Click' Chemistry. *Polym. Chem.* **2014**, *5*, 6318−6324.
(47) Ledin, P. A.; Tkachenko, I. M.; Xu, W.; Choi, I.; Shevchenko, V. V.; Tsukruk, V. V. Star-Shaped Molecules with Polyhedral Oligomeric Silsesquioxane Core and Azobenzene Dye Arms. *Langmuir* **2014**, *30*, 8856−8865.
(48) McConney, M. E.; Singamaneni, S.; Tsukruk, V. V. Probing Soft Matter with the Atomic Force Microscopies: Imaging and Force Spectroscopy. *Polym. Rev.* **2010**, *50*, 235−286.
(49) Hagemann, H. J.; Gudat, W.; Kunz, C. Optical Constants From the Far Infrared to the X-ray Region: Mg, Al, Cu, Ag, Au, Bi, C, and $A1_2O_3$. *J. Opt. Soc. Am.* **1975**, *65*, 742−744.
(50) Zhou, J.; Zhao, Y.; Yu, K.; Zhou, X.; Xie, X. Synthesis, Thermal Stability and Photoresponsive Behaviors of Azobenzene-Tethered Polyhedral Oligomeric Silsesquioxanes. *New. J. Chem.* **2011**, *35*, 2781−2792.
(51) Chi, H.; Mya, K. Y.; Lin, T.; He, C.; Wang, F.; Chin, W. S. Thermally Stable Azobenzene Dyes through Hybridization with POSS. *New. J. Chem.* **2013**, *37*, 735−742.

DOI: 10.1021/am508993z
ACS Appl. Mater. Interfaces 2015, 7, 4902−4912

(52) Miniewicz, A.; Girones, J.; Karpinski, P.; Mossety-Leszczak, B.; Galina, H.; Dutkiewicz, M. Photochromic and Nonlinear Optical Properties of Azo-Functionalized POSS Nanoparticles Dispersed in Nematic Liquid Crystals. *J. Mater. Chem. C* **2014**, *2*, 432−440.
(53) Su, X.; Guang, S.; Xu, H.; Liu, X.; Li, S.; Wang, X.; Deng, Y.; Wang, P. Controllable Preparation and Optical Limiting Properties of POSS-Based Functional Hybrid Nanocomposites with Different Molecular Architectures. *Macromolecules* **2009**, *42*, 8969−8976.
(54) Kawai, T.; Umemura, J.; Takenaka, T. Uv Absorption-Spectra of Azobenzene-Containing Long-Chain Fatty-Acids and Their Barium Salts in Spread Monolayers and Langmuir-Blodgett Films. *Langmuir* **1989**, *5*, 1378−1383.
(55) Sasaki, T.; Ikeda, T.; Ichimura, K. Photoisomerization and Thermal-Isomerization Behavior of azobenzene Derivatives in Liquid-Crystalline Polymer Matrices. *Macromolecules* **1993**, *26*, 151−154.
(56) Tanchak, O. M.; Barrett, C. J. Light-Induced Reversible Volume Changes in Thin Films of Azo Polymers: The Photomechanical Effect. *Macromolecules* **2005**, *38*, 10566−10570.
(57) Toccafondi, C.; Occhi, L.; Cavalleri, O.; Penco, A.; Castagna, R.; Bianco, A.; Bertarelli, C.; Comoretto, D.; Canepa, M. Photochromic and Photomechanical Responses of an Amorphous Diarylethene-Based Polymer: A Spectroscopic Ellipsometry Investigation of Ultrathin Films. *J. Mater. Chem. C* **2014**, *2*, 4692−4698.
(58) Tao, A.; Sinsermsuksakul, P.; Yang, P. Tunable Plasmonic Lattices of Silver Nanocrystals. *Nat. Nanotechnol.* **2007**, *2*, 435−440.
(59) Mahmoud, M. A.; Tabor, C. E.; El-Sayed, M. A. Surface-Enhanced Raman Scattering Enhancement by Aggregated Silver Nanocube Monolayers Assembled by the Langmuir-Blodgett Technique at Different Surface Pressures. *J. Phys. Chem. C* **2009**, *113*, 5493−5501.
(60) König, T.; Kodiyath, R.; Combs, Z. A.; Mahmoud, M. A.; El-Sayed, M. A.; Tsukruk, V. V. Silver Nanocube Aggregates in Cylindrical Pores for Higher Refractive Index Plasmonic Sensing. *Part. Part. Syst. Charact.* **2014**, *31*, 274−283.
(61) Chen, H. J.; Kou, X. S.; Yang, Z.; Ni, W. H.; Wang, J. F. Shape- and Size-Dependent Refractive Index Sensitivity of Gold Nanoparticles. *Langmuir* **2008**, *24*, 5233−5237.
(62) Ahamad, N.; Bottomley, A.; Ianoul, A. Optimizing Refractive Index Sensitivity of Supported Silver Nanocube Monolayers. *J. Phys. Chem. C* **2012**, *116*, 185−192.
(63) Mayer, K. M.; Hafner, J. H. Localized Surface Plasmon Resonance Sensors. *Chem. Rev.* **2011**, *111*, 3828−3857.
(64) Mahmoud, M. A.; Chamanzar, M.; Adibi, A.; El-Sayed, M. A. Effect of the Dielectric Constant of the Surrounding Medium and the Substrate on the Surface Plasmon Resonance Spectrum and Sensitivity Factors of Highly Symmetric Systems: Silver Nanocubes. *J. Am. Chem. Soc.* **2012**, *134*, 6434−6442.
(65) König, T.; Tsukruk, V. V.; Santer, S. Controlled Topography Change of Subdiffraction Structures Based on Photosensitive Polymer Films Induced by Surface Plasmon Polaritons. *ACS Appl. Mater. Interfaces* **2013**, *5*, 6009−6016.
(66) Müller, M. B.; Kuttner, C.; König, T. A. F.; Tsukruk, V. V.; Förster, S.; Karg, M.; Fery, A. A Plasmonic Library Based on Substrate-Supported Gradiential Plasmonic Arrays. *ACS Nano* **2014**, *9*, 9410−9421.
(67) Haggui, M.; Dridi, M.; Plain, J.; Marguet, S.; Perez, H.; Schatz, G. C.; Wiederrecht, G. P.; Gray, S. K.; Bachelot, R. Spatial Confinement of Electromagnetic Hot and Cold Spots in Gold Nanocubes. *ACS Nano* **2012**, *6*, 1299−1307.
(68) de Fornel, F. *Evanescent Waves: From Newtonian Optics to Atomic Optics*; Springer: Berlin, 2001.
(69) Knight, M. W.; Wu, Y.; Lassiter, J. B.; Nordlander, P.; Halas, N. J. Substrates Matter: Influence of an Adjacent Dielectric on an Individual Plasmonic Nanoparticle. *Nano Lett.* **2009**, *9*, 2188−2192.

DOI: 10.1021/am508993z
ACS Appl. Mater. Interfaces 2015, 7, 4902−4912